Field-Effect Transistor Based Detectors for Power Monitoring of THz Quantum Cascade Lasers

Justinas Zdanevičius, Dovilė Čibiraitė, Kęstutis Ikamas, *Graduate Student Member, IEEE*, Maris Bauer, Jonas Matukas, Alvydas Lisauskas, *Member, IEEE*, Heiko Richter, Till Hagelschuer, Viktor Krozer, *Senior Member, IEEE*, Heinz-Wilhelm Hübers, and Hartmut G. Roskos

***Abstract*—We report on circuit simulation, modeling, and characterization of field-effect transistor based terahertz (THz) detectors (TeraFETs) with integrated patch antennas for discrete frequencies from 1.3 to 5.7 THz. The devices have been fabricated using a standard 90-nm CMOS technology. Here, we focus in particular on a device showing the highest sensitivity to 4.75-THz radiation and its prospect to be employed for power monitoring of a THz quantum cascade laser used in a heterodyne spectrometer GREAT (German REceiver for Astronomy at Terahertz frequencies). We show that a distributed transmission line based detector model can predict the detector's performance better than a device model provided by the manufacturer. The integrated patch antenna of the TeraFET designed for 4.75 THz has an area of $13 \times 13\ \mu\text{m}^2$ and a distance of 2.2 μm to the ground plane. The modeled radiation efficiency at the target frequency is 76% with a maximum directivity of 5.5, resulting in an effective area of 1750 μm^2. The detector exhibits an area-normalized minimal noise-equivalent power of 404 pW/$\sqrt{\text{Hz}}$ and a maximum responsivity of 75 V/W. These values represent the state of the art for electronic detectors operating at room-temperature and in this frequency range.**

Manuscript received June 29, 2018; accepted September 3, 2018. Date of publication November 15, 2018; date of current version December 11, 2018. This work was supported in part by the Research Council of Lithuania under Contract S-LAT-17-3 and in part by the Marie Curie European Training Networks ITN CELTA under Contract 675683. *(Corresponding author: Alvydas Lisauskas.)*

J. Zdanevičius, J. Matukas, and A. Lisauskas are with the Institute of Applied Electrodynamics and Telecommunications, Vilnius University, Vilnius LT-10257, Lithuania (e-mail: justinas.zet@gmail.com; jonas.matukas@ff.vu.lt; lisauskas@physik.uni-frankfurt.de).

D. Čibiraitė and H. G. Roskos are with the Physikalisches Institut, Johann Wolfgang Goethe-Universität Frankfurt, Frankfurt D-60438, Germany (e-mail: cibiraite@physik.uni-frankfurt.de; roskos@physik.uni-frankfurt.de).

K. Ikamas is with the Institute of Applied Electrodynamics and Telecommunications, Vilnius University, Vilnius LT-10257, Lithuania, and also with the General Jonas Žemaitis Military Academy of Lithuania, Vilnius LT-10322, Lithuania (e-mail: kestutis.ikamas@ff.vu.lt).

M. Bauer is with the Physikalisches Institut, Johann Wolfgang Goethe-Universität Frankfurt, Frankfurt D-60438, Germany, and also with the Center for Materials Characterization and Testing, Fraunhofer ITWM, Kaiserslautern D-67663, Germany (e-mail: maris.bauer@itwm.fraunhofer.de).

H. Richter, T. Hagelschuer, and H.-W. Hübers are with the Institute of Optical Sensor Systems, German Aerospace Center (DLR), Berlin D-12489, Germany (e-mail: heiko.richter@dlr.de; Till.Hagelschuer@dlr.de; heinz-Wilhelm.huebers@dlr.de).

V. Krozer is with the Physikalisches Institut, Johann Wolfgang Goethe-Universität Frankfurt, Frankfurt D-60438, Germany, and also with the Ferdinand-Braun-Institut, Leibniz-Institut für Höchstfrequenztechnik, Berlin D-12489, Germany (e-mail: krozer@physik.uni-frankfurt.de).

Color versions of one or more of the figures in this paper are available online at http://ieeexplore.ieee.org.

Digital Object Identifier 10.1109/TTHZ.2018.2871360

***Index Terms*—German REceiver for Astronomy at Terahertz frequencies (GREAT), plasmonic detection, Stratospheric Observatory for Infrared Astronomy (SOFIA), terahertz (THz) detectors, THz quantum cascade laser (QCL).**

I. Introduction

HIGH-RESOLUTION and high-sensitivity heterodyne-based spectroscopic observations for astronomy require stable local oscillator (LO) sources operating in the terahertz (THz) frequency range. For example, a major coolant of the dense interstellar medium, the neutral atomic oxygen, has a fine-structure line at 4.7448 THz. Monitoring of this line became an important tool in order to understand the formation of massive young stars [1].

One of the monitoring laboratories is the Stratospheric Observatory for Infrared Astronomy (SOFIA). For high-resolution and high-sensitivity measurements at various frequencies, the heterodyne spectrometer GREAT (German REceiver for Astronomy at Terahertz frequencies) employs multiplied microwave sources in all channels, except the highest one at 4.75 THz where a solution of this kind is not available. Instead, a quantum cascade laser (QCL) is employed to cover this frequency, which emerged as an alternative THz source solution to the gas lasers for such measurements [2], [3].

While the mixer employed in the GREAT spectrometer can itself provide information on the impinging THz power, a continuous monitoring of the THz QCL power with an independent easy-to-operate reference detector is desirable. The real-time monitoring of the QCL power allows a straightforward realization of a corresponding control loop, which is independent from the rest of the complex GREAT instrument and only related to the QCL. It can easily make use of the big amount of QCL power dumped after the beam splitter ($>$1 mW). Commercial devices operating at room-temperature conditions, such as a Golay cell [4] or pyroelectric detectors [5], require the implementation of chopping techniques, which is undesirable because of space constraints. Planar antenna-integrated zero-bias Schottky diodes could offer one of the possibilities; yet, the best available data indicate a strong sensitivity roll-off in the frequency range from 100 GHz to 1 THz [6]. GaAs Schottky diodes, which are optimized for the target frequency range [7], [8], possess high $1/f$ noise and are not suitable for continuous-wave (CW) power measurements.

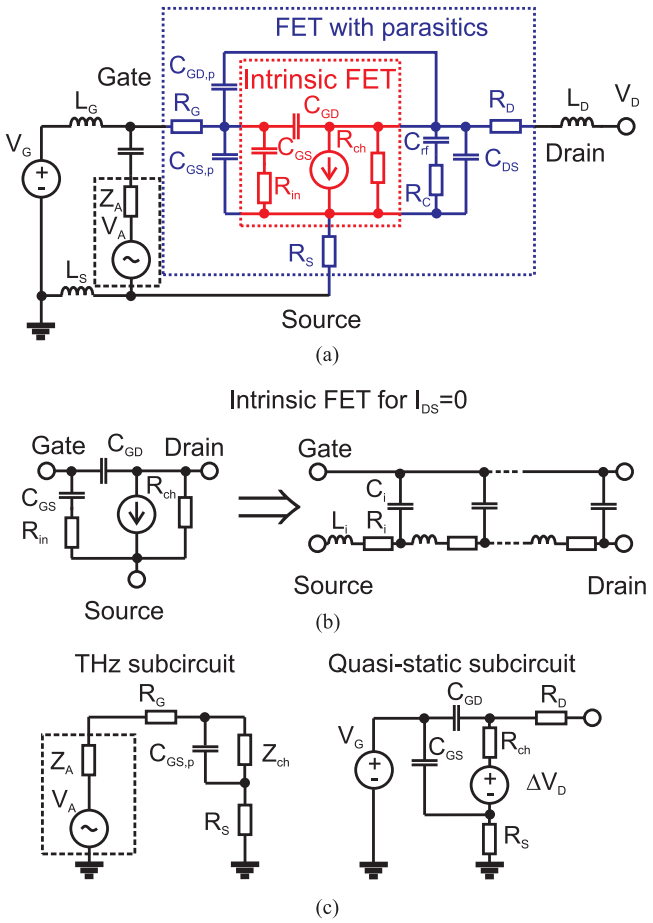

Fig. 1. (a) Electronic circuit of silicon CMOS-based THz detector with marked parts: Intrinsic FET channel (red), FET parasitic parts (purple), and the antenna (black). (b) TL circuit describing the intrinsic FET channel. (c) Simplified high-frequency (left) and low-frequency (right) electronic circuits.

Recently, it was reported that field-effect transistor based THz detectors (TeraFETs) can offer an alternative solution for operation in a specified frequency range [9] and, in particular, in application with THz QCLs [10], [11]. Here, we continue with our explorations and discuss on the design and implementation of TeraFETs for upper THz frequency range, showing the prospects of low noise-equivalent power (NEP) TeraFETs to monitor the power THz QCLs in the CW mode.

We organize this paper in the following way: In Section II, we present the details of our detector modeling and implementation. In Section III, we present the details of our measurement setup, and in Section IV, we discuss our detector spectral characteristics, linearity of response, electrical noise characteristics, and also the sensitivity of the detectors.

II. Detector Implementation

A schematic circuit for a generalized TeraFET is shown in Fig. 1(a). The antenna is described by the equivalent voltage source in series with the connected impedance Z_A. Since the antenna is used for receiving the THz radiation, voltage V_A represents the open-circuit voltage, which can be expressed through the maximum available power $P_{\max} = V_a^2/(8\mathrm{Re}(Z_A))$ [12], [13]. There are different models that describe the operation of a field-effect transistor (FET) depending on the biasing conditions and frequencies. For these purposes, one can use either a model description, which is provided by the manufacturer of electronic components, or technology-typical modeling parameters [14] or, where the standard description is not satisfactory (e.g., the operation in THz frequency range) work with analytic or customized circuit-level descriptions.

In the following treatment, we rely on the assumption that detection occurs only in the intrinsic FET region, and the influence of a parasitic transistor part is unwanted and diminishes the performance of the detector. For the circuit-level analysis described here, we use two modeling methods that account for parasitic effects: A model that is supplied by a foundry for the used technology and an analytical transmission line (TL) based model.

A. Analytic TL Based Detector Model

The analytical approximation of TeraFETs differs from the foundry-based model mainly in the description of the electronic transport in the channel region. It was recognized that transport equations used in physical modeling at high frequencies are equivalent to propagation through TLs [15]–[17]. Moreover, for THz detectors with unbiased channels, a TL analogy [see Fig. 1(b)] is expected to describe the intrinsic FET better than the lumped element description, even if the elements C_{GS}, R_{in}, C_{GD}, and R_{ch} are refined by their nonquasi-static approximates [18].

The channel of the transistor at THz frequencies can be described as a TL with resistance $R_i = (qn\mu W)^{-1}$, inductance $L_i = R_i\tau$, and capacitance $C_i = qW\partial n/\partial V_G$ defined per unit length. Here, n is the charge density in the channel, q is the elementary charge, W is the width of the channel, μ is the carrier mobility, τ is the carrier scattering time, and V_G is the gate voltage. This representation corresponds to an electronic circuit of charge-density (plasma) waves in the transistor channel.

The general circuit of the detector can further be simplified by separately treating the high-frequency and low-frequency (quasi-static) cases, as shown in Fig. 1(c). To calculate the responsivity $\Re_V$, we start with the simplified hydrodynamic channel-transport model of Dyakonov and Shur [19]. The voltage swing applied between the gate and source terminals at the interface to the channel excites carrier density waves (plasma waves), which propagate through the channel with velocity s given by

$$s = \sqrt{\frac{qn}{m}\left(\frac{\partial n}{\partial V_G}\right)^{-1}}. \tag{1}$$

In the simplified transport picture, the average charge density in the channel is inversely proportional to the dc resistance R_{ch} of the gated part of the channel; therefore, the quantity $n\partial V_G/\partial n$ can be expressed from the measured dc resistance R_{dc}, i.e., $n\partial V_G/\partial n = -R_{\mathrm{ch}}\partial V_G/\partial R_{\mathrm{ch}} \equiv -(\partial \ln R_{\mathrm{ch}}/\partial V_G)^{-1}$, with $R_{\mathrm{ch}} = R_{\mathrm{dc}} - R_S - R_D$. For the small-signal excitation conditions with the onto intrinsic device delivered voltage amplitude V_{THz}, one can follow the solution method proposed by Dyakonov and Shur [19] and Boppel *et al.*

[20] and find the induced voltage ΔV as follows:

$$\Delta V = \frac{qV_{\mathrm{THz}}^2}{4ms^2} f(\omega,\tau) = -\frac{V_{\mathrm{THz}}^2}{4}\frac{\partial \ln R_{\mathrm{ch}}}{\partial V_G} f(\omega,\tau). \quad (2)$$

Here, $m = 0.26m_e$ is the effective mass of electrons in Si (m_e is the free-electron mass), τ is their momentum scattering time, ω is the angular frequency of the THz wave, and $f(\omega,\tau) = 1 + 2\omega\tau/\sqrt{1+(\omega\tau)^2}$ is the detection efficiency factor describing the conversion ability relative to that of low-frequency resistive mixing [21] in a nonresonant case ($s\tau/L \ll 1$, L is the gate length).

The responsivity of the detector is defined as the ratio of the induced voltage ΔV to the impinging power P_{THz}, i.e., $\Re_V = \Delta V/P_{\mathrm{THz}}$. The power, which is used to characterize $P_{\max}$ of the antenna, is equal to $P_{\mathrm{THz}}\eta$, where η jointly combines the antenna efficiency factor and other possible optical coupling loss mechanisms. We introduce an amplitude attenuation factor $H = |V_{\mathrm{THz}}|/|V_a|$, which occurs upon the signal transfer from the antenna to the transistor's channel. Considering the parasitic device elements shown in the THz subcircuit [see Fig. 1(c)], i.e., R_G, R_S, and the high-frequency capacitive conductance $C_{\mathrm{GS},p}$, the resulting mathematical expression for the voltage attenuation factor is as follows:

$$H = \left| \frac{Z_{\mathrm{ch}} \parallel Z_p}{Z_{\mathrm{ch}} \parallel Z_p + Z_A + R_G + R_S} \right|. \quad (3)$$

Here, $Z_{\mathrm{ch}} \parallel Z_p$ denotes the resultant impedance for the parallel-connected channel impedance Z_{ch} and the shunting capacitance $Z_p = (i\omega C_{\mathrm{GS},p})^{-1}$ subsuming fringe and overlap capacitance, Z_A is the antenna impedance, and R_G and R_S are the gate and source resistances, respectively.

This, finally, leads to the voltage responsivity of plasmonic FET-based detectors, predictable from the measured static device characteristics and modeled high-frequency parameters as follows:

$$\Re_V = -\frac{1}{4}\frac{\partial \ln R_{\mathrm{ch}}}{\partial V_G}\left[1 + \frac{2\omega\tau}{\sqrt{1+(\omega\tau)^2}}\right] 8\mathrm{Re}(Z_A)H^2\eta. \quad (4)$$

The impedance of the channel Z_{ch} under the condition of ac-shorted gate and drain terminals can be described via the characteristic impedance of the TL as follows:

$$Z_{\mathrm{ch}} = \sqrt{\frac{R_i + i\omega L_i}{i\omega C_i}} \tanh(\gamma L) \quad (5)$$

where $\gamma = \sqrt{(R_i + i\omega L_i)i\omega C_i}$ is the propagation constant. In another limiting case of an ac open drain, a $\tanh(kL)$ function changes to $\coth(kL)$. However, under the condition of strong damping for plasma waves and $|kL| \gg 1$, both functions asymptotically approach unity. We assume the parasitic impedance $Z_p = (i\omega C_{\mathrm{GS},p})^{-1}$, with $C_{\mathrm{GS},p}$ assumed to be half of the overlap capacitance C_{ov} between the source and gate terminals. With $L = 0.1$ μm, $W = 0.4$ μm, $d = 2.4$ nm, and $\epsilon_r = 4.3$, $C_{\mathrm{ov}} \approx 0.1\ \mathrm{LW}\epsilon_r\epsilon_0/d = 63.5$ aF.

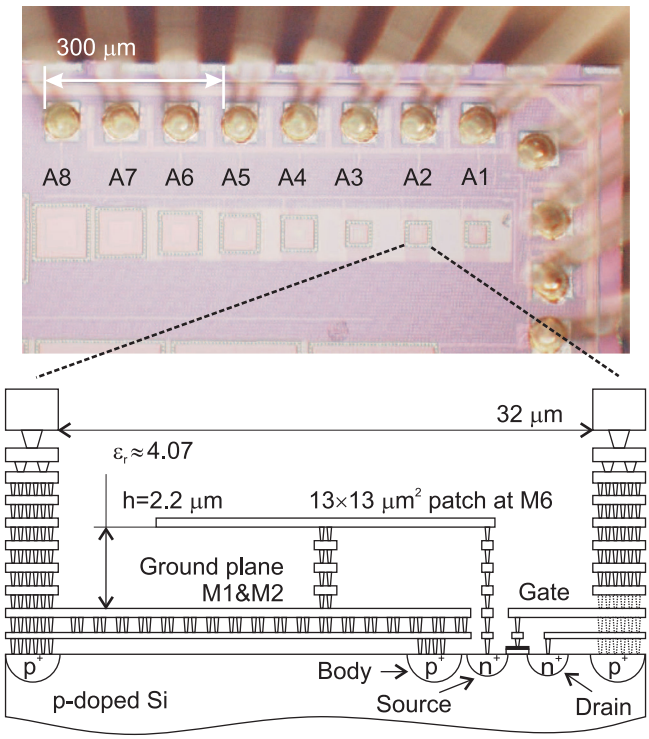

Fig. 2. Detector line and a single detector design. The detector line (above) shows different detectors (coded A1–A8) with various antenna sizes and transistors. The detector design (bottom) shows all the metal layers, starting from M9 down to M1, where the ground plane is placed. The source, gate, and drain show the transistor contacts. Elements in the view are not to scale.

TABLE I
ANTENNA SIMULATION PARAMETERS

Pixel	Patch Size (μm^2)	Box Size (μm^2)	Height (μm)	Res. Frequency (THz)	Directivity	Efficiency (%)
A1	10×10	32×32	2.2	5.75	6.64	62
A2	13×13	32×32	2.2	4.6	5.79	76
A3	17×17	32×32	2.84	3.56	6.46	76
A4	19×19	50×50	2.84	3.17	6.42	79
A5	23×23	56×56	2.84	2.8	5.32	71
A6	32×32	62×62	3.6	2.0	4.7	63
A7	41×41	74×74	3.6	1.64	4.76	53
A8	52×52	86×86	3.6	1.35	5.23	43

B. Detector Layout and Fabrication

The detectors have been designed for a standard 90-nm complementary metal–oxide–silicon (CMOS) technology of Taiwan Semiconductor Manufacturing Company. The detector couples THz radiation with the *N*-channel FET through the patch antenna. Devices with various antenna sizes were designed (see Fig. 2). In all devices, we used the same channel length $L = 100$ nm and width $W = 400$ nm. Table I presents important geometrical parameters of the antennas, as well as simulation results obtained with the CST Microwave Studio software. It comprises the dimensions of the patch, height between the patch and the ground plane, dimensions of the metallic cup, resultant resonance frequency, directivity, and radiation efficiency

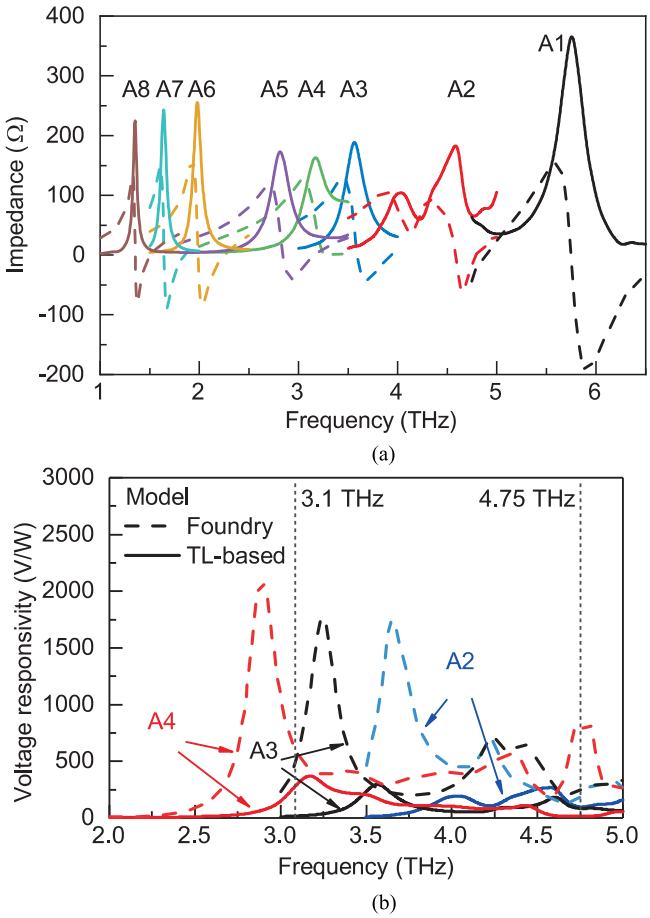

Fig. 3. (a) Simulated antenna impedance spectra for antennas used with A1–A8 devices. The real and imaginary parts of the impedance are presented using solid lines and dashed lines, respectively. (b) Modeled frequency response for A2, A3, and A4 devices. Solid lines correspond to analytic TL-based calculations, whereas dashed lines result from the foundry-provided model. Two vertical dashed lines mark frequencies of two THz QCLs used in this study.

at resonance. Simulated antenna impedance spectra are shown in Fig. 3(a).

Fig. 3(b) depicts frequency responses for A2, A3, and A4 devices. Solid lines correspond to analytic TL-based calculations, whereas dashed lines result from the foundry-provided model. It is notable that the foundry model predicts higher response at much lower frequencies compared with the resonant frequency of the antenna and with predictions from TL-based description. The discrepancy might originate from the fact that a foundry model that is validated at frequencies below 100 GHz tends to overestimate capacitive shunting at frequencies exceeding 1 THz. Therefore, the more efficient rectification is expected when the antenna exhibits a strong inductive behavior. It is worth noting that the detector with the same parameters can be modeled using the device model supplied for the more advanced 65-nm CMOS technology (data not shown here). In this case, it would predict the maximum responsivity at similar frequencies as our TL model. We can just speculate that a 65-nm model accounts better for nonquasi-static effects, thus supporting the rationale of the analytical model.

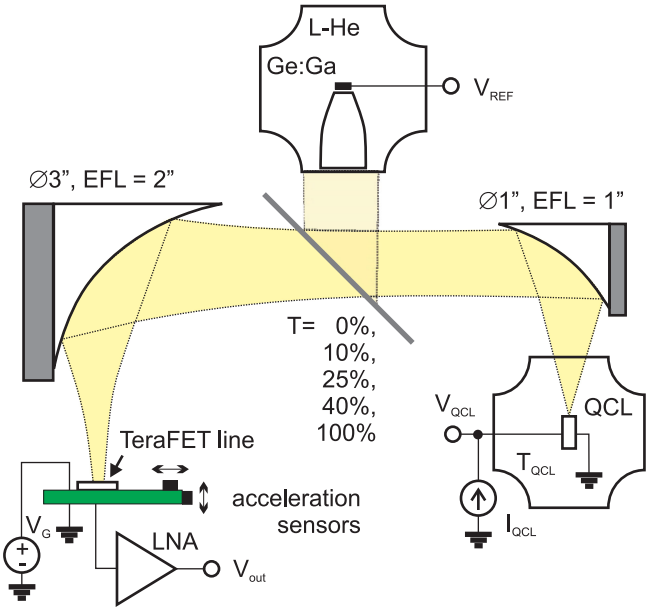

Fig. 4. Measurement setup. The THz radiation emitted by the QCL is collimated with a 1-in EFL parabolic mirror and, then, divided into two parts: One part of the beam is guided to a Ge:Ga detector, and the transmitted part is focused onto the CMOS detector using a 2-in EFL parabolic mirror. The CMOS detector also contains acceleration sensors. Detected signals from the acceleration sensors, the QCL, and both detectors are recorded.

III. Measurement Setup

The experiment has been conducted with a LO development platform, which is an exact copy of the platform used in SOFIA. The experimental setup is shown in Fig. 4.

The QCL is mounted on the cold finger of the two-staged Stirling cryocooler (model Ricor K535) [2]. The second stage of the cooler is doubled in symmetrical manner to avoid large mechanical vibrations. The heat sink of the cryocooler is altered by changing the default cooling fins to the custom ones in order to meet the standards of the SOFIA devices. The temperature sensor and the heater are attached to the QCL, and a controlling system based on field programmable gate array is used for temperature stabilization. During the experiment, the cooling system was capable of maintaining the QCL's temperature of 49 K.

The THz radiation emitted by the QCL is collimated with a 1-in effective focal length (EFL) parabolic mirror and, then, divided into two parts using a 40%/60% (transmission/reflection) beamsplitter. One part of the beam is directed onto a Ge:Ga detector with Winston cone coupling optics, whereas the transmitted part is focused onto the CMOS detector using a 2-in EFL parabolic mirror. The beamsplitter is self-made by evaporating a thin layer of Cr on a 4-μm-thick polypropylene foil. For power attenuation, we use two separate items with transmissions of 40% and 25%, whereas 10% attenuation was achieved by combining both. In order to investigate the role of mechanical vibrations produced by the cryocooler, we place three acceleration sensors (to capture three directions of movement) on the holder of the CMOS detector. In addition to detected signals from the TeraFET, the reference detector, and acceleration sensors, we

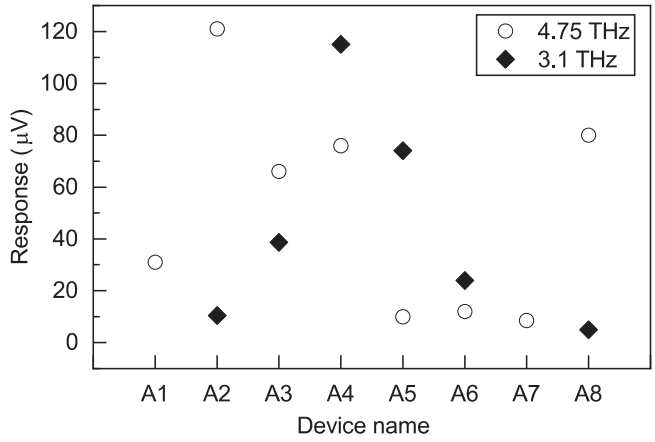

Fig. 5. Response voltages at the maximum voltage responsivity for A1–A8 devices to 3.1 and 4.75 THz radiation.

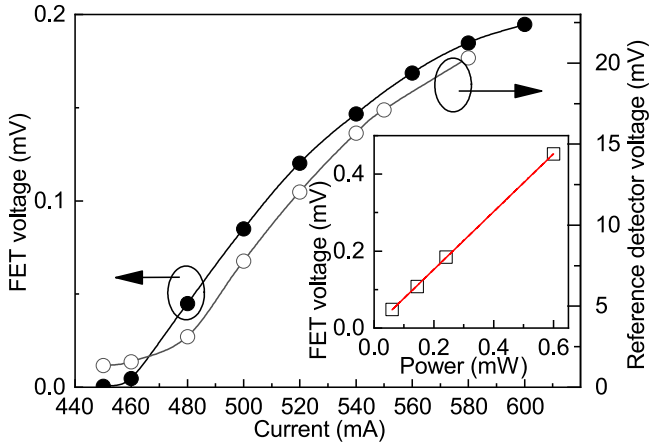

Fig. 6. Response of the TeraFET A2 as a function of the 4.75-THz QCL bias current. The inset shows the linearity of the response for bias current $I_{QCL} = 600$ mA and at different levels of attenuation.

simultaneously recorded V_{QCL} and T_{QCL} using a multichannel 24-bit National Instruments data acquisition system.

The measurement with room-temperature CMOS TeraFET does not need any chopping or other THz signal modulation of the QCL power fluctuations; therefore, the measurements were conducted in the CW mode at room-temperature. For the responsivity measurements, a lock-in amplifier was used with the QCL current modulation as the reference signal.

IV. Results and Discussion

A. Detector Spectral Characteristics

Response voltages at the maximum voltage responsivity for A1–A8 devices to 3.1 and 4.75 THz radiation are depicted in Fig. 5. Results clearly indicate that the highest response is observed with devices A4 and A2, for which the antenna resonance frequencies are close to the frequencies of THz QCLs. In addition to fundamental resonances, a strong response to 4.75-THz radiation can be observed with the device A8, resulting in the excitation of higher order resonance in the patch antenna.

One of the best indicators for the comparison of model prediction can be the performance of A3 detector at 3.1 THz. Simulating detector characteristics with the foundry model for the transistor results in this detector having the best relative performance, whereas the TL-model predicts a relatively low response. Experimental data indicate that at this frequency, the most sensitive device is A4, thus favoring earlier discussed analytically derived TL-model predictions. However, the relatively high response of device A3 points out that further tuning of parasitic circuit elements is advantageous. This is planned in future experiments, which will involve additional THz QCLs with different emission frequencies.

B. Linearity of the Response

Fig. 6 depicts the response of the TeraFET A2 as a function of 4.75-THz QCL bias current. The right axis presents simultaneous measurement with the reference, the cryogenically cooled Ge:Ga detector. These curves resemble each other well, except for the low bias currents. Such discrepancies are due to the fact that despite its superior sensitivity, the impurity-band-based detector has a strong dc output component (approximately 1.6 V), whereas the THz-induced signal change was maximally 20 mV. Therefore, due to a slight change in the background level during the long duration of the experiment, the power estimation performed with the reference detector was less accurate than that with the TeraFET. For the measurements of the linearity of the response, we employed self-made attenuators based on transmission through a thin metallic surface evaporated on a 4-μm-thick polypropylene foil. The calibration has been performed with tunable electronic sources in the frequency range of 200–700 GHz. The symbols shown in the inset correspond to the THz response for bias current $I_{QCL} = 600$ mA and at four different levels of attenuation, i.e., 0 %, 60 %, 75 %, and 90 %. The line is the linear fit indicating that under the experimental conditions, the detectors operate in the linear (power) detection regime.

C. Electrical Noise

Fig. 7 depicts the spectra of voltage fluctuation spectral density of the input-referred voltage of TeraFET V_{out} for different THz attenuation ratios (blocked, transmission of 40% and 100%) when the THz QCL is biased with $I_{QCL} = 580$ mA. The dashed line indicates the thermal noise level of 18 nV/$\sqrt{\text{Hz}}$ of the 20-kΩ resistor. These spectra exhibit a thermally limited baseline with the roll-off frequency at 10 kHz originating from the external 6-dB/oct low-pass filter, small $1/f$ noise contribution, and a lot of strong but narrow spectral components that couple with the detector output from the environment. Low-frequency components at 45 Hz and their multiplicative originate from the vibration of cables induced by the cryocooler and can be strongly suppressed by using an integrated low-noise amplifier within the detector package. A considerably high channel impedance of 20 kΩ allows easy integration of low-noise amplifiers based on discrete components or integrated circuits with convenient 4-nV/$\sqrt{\text{Hz}}$ input-referred voltage fluctuation

TABLE II
THz Detector Performance Comparison

Device	Technology	Detection Mechanism	Frequency (THz)	$\Re_V$ (V/W)	NEP (pW/$\sqrt{\text{Hz}}$)	Modulation Frequency (Hz)	Effective Area (μm^2)	Ref.
Golay Cell	-	Optoacoustic	0.02-20	10k with amp.	10^4	12.5	$2.83 \cdot 10^7$	[25]
Golay Cell	-	Optoacoustic	0.04-20	100k with amp.	120 (typical)	20	$2.83 \cdot 10^7$	[4]
Pyroelectric	-	Thermal	3-6.6	450	600 [a]	5	$7.8 \cdot 10^5$	[5]
Thermopile	SiN membrane	Thermal	1.6-4.3	-	1000	<200	1000×1000	[26]
μBolometer	VOx	Thermal	2.51, 4.28	-	<10 [b]	30	23.5×23.5	[27]
μBolometer	VOx	Thermal	2.54, 4.25	-	14.4 [b]	30	52×52	[28]
μBolometer	a-Si	Thermal	2.5	12.6M with amp.	6 [b]	25	50×50	[29]
HEB	AlGaN/GaN 2DEG	Thermal	2.55	40 mA/W	5000	-	4405 [d]	[30]
MOSFET	0.18-μm SOI-CMOS	Thermal	0.6-1.2	100 mA/W	25	10	250×250	[31]
NMOS	150-nm CMOS	Electronic	8.4	1	1474	30	-	[32]
NMOS	90-nm CMOS	Electronic	4.25	230	110	131	1691 [d]	[9]
SBD	130-nm CMOS	Electronic	4.92	383	4950 [c]	300	1574	[33]
SBD	130-nm CMOS	Electronic	9.74	14	2000 [c]	80	547	[33]
SBD	GaAs	Electronic	2.54	60	330 [c]	100k	corner-cube	[7]
SBD	GaAs	Electronic	5.3	10	-	-	corner-cube	[8]
NMOS	90-nm CMOS	Electronic	4.75	75	404	331	1750	this work

[a]Devices for 3–6.6 THz range are supplied with an Si window with ≈ 50% transmission; thus, the datasheet values are scaled by the factor of 2.
[b]The NEP is estimated from the minimum detectable power (MDP) per frame. NEP = MDP/$\sqrt{f_{\text{mod}}}$.
[c]The NEP is specified for the shot-noise limit above the corner frequency of $1/f$ noise, which dominates at low modulation frequencies.
[d]Calculated from specified values using the relation $A_{\text{eff}} = D\lambda^2/(4\pi)$.

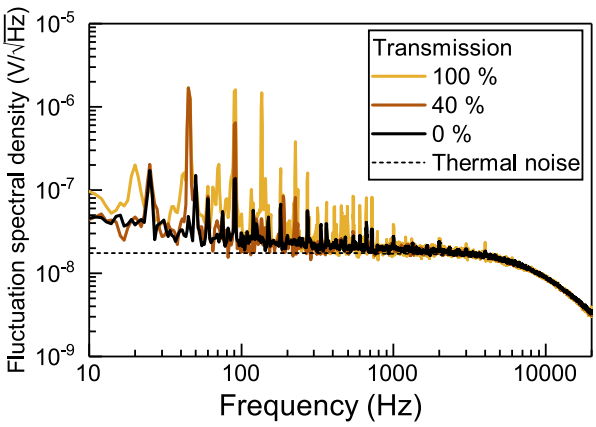

Fig. 7. Spectra of voltage fluctuation spectral density for the input-referred voltage of A2 TeraFET V_G biased to 0.45 V for different THz signal attenuation ratios when the 4.75-THz QCL is biased with $\text{I}_{\text{QCL}} = 580$ mA. The dashed line represents the calculated thermal noise with a low-pass filter ($f_{3\text{dB}} = 10$ kHz).

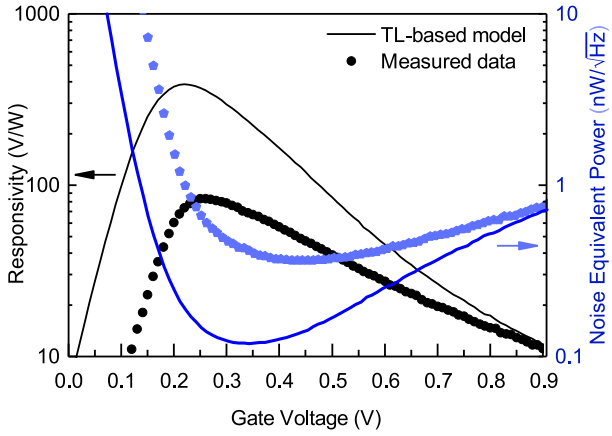

Fig. 8. Responsivity (left axis) and NEP (right axis) as a function of the bias voltage for A2 TeraFET at 4.75 THz.

spectral density [22], which introduces additional noise contribution only by 2.5%. The corner frequency of $1/f$ noise for the detector–amplifier system lies at about 30 Hz.

We also found that in the case of strong focusing of THz radiation onto the detector and back-coupling of radiation into the QCL, both the intensity of THz radiation and the bias voltage V_{QCL} start exhibiting strongly correlated low-frequency fluctuations (for details, see [11]). However, the weak feedback of a back-coupled signal can find practical applications in reflection imaging and gas spectroscopy [23], [24], and the increase in the amplitude of low-frequency fluctuations limits the sensitivity of the detector intended to work in the dc regime. Assuming that back-reflections will be suppressed, in general, the noise of the detector does not depend on the QCL current and is limited by the thermal noise. Therefore, for the effective measurement bandwidth of 1 Hz, a signal-to-noise ratio (*S*/*N*) of 40 dB is granted when a fraction of the power (approximately 250 μW) is directed onto the detector.

D. Sensitivity

Based on experimentally measured response and noise characteristics, as depicted in Fig. 8, we present the responsivity and the thermal noise limited NEP of TeraFET A2 at target 4.75-THz frequency (symbols). The dashed lines show the predictions resulting from previously described analytic model (see Section II-A). The effective area of the antenna was estimated by the relation $A_{\text{eff}} = D\lambda^2/(4\pi)$, with D and λ representing the directivity and the wavelength in free space, respectively. With the modeled value $D = 5.5$ at 4.75 THz, we arrive at $A_{\text{eff}} = 1750$ μm^2, which is about 1.7 times larger than the area of the implemented metal cup. In the calibration measurement, the beam profile of QCL radiation at the detector's plane was recorded with the microbolometric camera and estimated to be

1.3 mm for horizontal full-width-at-half-maximum (FWHM) and 0.8 mm for vertical FWHM. From the total power and under the assumption of Gaussian beam form, we have estimated the power delivered to the detector. The detector reaches a maximum responsivity of 75 V/W. The minimum NEP of 404 pW/$\sqrt{\text{Hz}}$ is achieved at a gate voltage of 0.45 V. Values reported here differ from those reported earlier [11] only by the ratio between modeled effective areas (1750 μm^2 instead of previously used 1600 μm^2). Comparing with theory predictions, we notice that both modeled and measured responsivities nearly coincide only for gate bias voltages near 0.9 V, whereas in the vicinity of the threshold voltage ($V_{\text{th}} = 0.43$ V), we did not observe as strong responsivity as should follow from our analytic predictions. It is possible that the discrepancy can originate either from the simplified description of the receiving antenna or from the identification of parasitic components or from the simplifications in the physical description of charge transport (i.e., omitted carrier heating [34], [35], a quasi-static description of charge carrier control by gate voltage [16], [34], etc.).

The state of the art for the room-temperature THz detectors operating in the frequency range of 1–10 THz is presented in Table II. For a long period of time, GaAs-based Schottky barrier diodes (SBDs) [7], [8] dominated this frequency range. Due to required biasing, these devices exhibit strong $1/f$ noise contribution; thus, the listed performance is achievable only in the shot-noise-limited regime for modulation frequencies typically exceeding 100 kHz. The successful demonstration of the operation of a standard infrared imager at 4.3 THz with a NEP value of 320 pW/$\sqrt{\text{Hz}}$ [36] launched the race between the manufacturers of microbolometer (μ Bolometer) cameras, and now, THz-tailored devices demonstrate unprecedented NEP values below 10 pW/$\sqrt{\text{Hz}}$ [27], [29]. One drawback of microbolometers could be their considerably long integration time, which is close to the inverse of the frame rate [27]. There are reports that single devices can have submicrosecond thermal response times [37]; these data are available only for devices optimized for 300 and 765 GHz. The device presented here continued on developments described in [9] and [32]. The reported performance values are in full competition with SBDs and commercial devices, such as Golay cells and pyroelectric devices, however, without the $1/f$-noise limitation and the necessity of chopping, thus fully complying with the requirements for application in monitoring THz QCL power in the GREAT spectrometer.

V. Summary

In summary, we present a series of TeraFETs with resonant patch antennas for detection at discrete frequencies from 1.3 to 5.7 THz. In particular, we concentrate on a device, which shows the highest sensitivity to 4.75 THz, and its prospect to be employed for power monitoring of the THz QCL used in the heterodyne spectrometer GREAT.

The TeraFET for 4.75 THz has the dimensions of the patch antenna as 13×13 μm^2 and the height to the ground plane as 2.2 μm. The modeled radiation efficiency at 4.75 THz is 76% with a maximum directivity of 5.5, resulting in an effective area of 1750 μm^2. The detector exhibits an area-normalized minimal NEP of 404 pW/$\sqrt{\text{Hz}}$ and a maximum responsivity of 75 V/W. These values are at the state-of-the-art level for electronic detectors operating at room-temperature and for this frequency range. We show that a TL-based detector model can better predict detector performance than the device model provided by the manufacturer.

Regarding the applicability of TeraFETs, we demonstrate that the detector for 4.75 THz has linear power dependence over the whole power range of the QCL and can monitor the intensity of THz QCL radiation using a fraction of the beam power (approximately 250 μW) with a *S/N* ratio of 40 dB. Since the TeraFET does not require chopping, it has an advantage over alternative room-temperature detectors and can be employed in a heterodyne instrument as a reference detector for real-time QCL power monitoring.

References

[1] R. T. Boreiko and A. L. Betz, "Heterodyne spectroscopy of the 63 μm OI line in M42," *Astrophysical J. Lett.*, vol. 464, pp. L83–L86, 1996.

[2] H. Richter *et al.*, "A compact, continuous-wave terahertz source based on a quantum-cascade laser and a miniature cryocooler," *Opt. Express*, vol. 18, no. 10, pp. 10177–10187, May 2010.

[3] H. Richter *et al.*, " 4.7-THz local oscillator for the GREAT heterodyne spectrometer on SOFIA," *IEEE Trans. Terahertz Sci. Technol.*, vol. 5, no. 4, pp. 539–545, Jul. 2015.

[4] *THz Golay cell detector datasheet for model gc-1p with HDPE window*, Tydex Inc. Jun. 14, 2018. [Online]. Available: http://www.tydexoptics.com

[5] *Pyroelectric detector datasheet for model sph-21*, Spectrum Detectors Inc. Jun. 14, 2018. [Online]. Available: http://www.crazyfingers.com/spectrum/products/pyroelectricDetectors/index.php

[6] M. Yahyapour *et al.*, "A flexible phase-insensitive system for broadband CW-terahertz spectroscopy and imaging," *IEEE Trans. Terahertz Sci. Technol.*, vol. 6, no. 5, pp. 670–673, Sep. 2016.

[7] V. G. Bozhkov, "Semiconductor detectors, mixers, and frequency multipliers for the terahertz band," *Radiophys. Quantum Electron.*, vol. 46, no. 8, pp. 631–656, 2003.

[8] T. Yasui, A. Nishimura, T. Suzuki, K. Nakayama, and S. Okajima, "Detection system operating at up to 7 THz using quasioptics and Schottky barrier diodes," *Rev. Scientific Instrum.*, vol. 77, no. 6, 2006, Art. no. 066102.

[9] M. Bauer *et al.*, "Antenna-coupled field-effect transistors for multispectral terahertz imaging up to 4.25 THz," *Opt. Express*, vol. 22, no. 16, pp. 19235–19241, Aug. 2014.

[10] K. Ikamas, A. Lisauskas, S. Boppel, Q. Hu, and H. G. Roskos, "Efficient detection of 3 THz radiation from quantum cascade laser using silicon CMOS detectors," *J. Infrared, Millimeter, Terahertz Waves*, vol. 38, pp. 1–6, Jun. 2017.

[11] J. Zdanevičius *et al.*, "TeraFET detector for measuring power fluctuations of 4.75-THz QCL-generated radiation," in *Proc. Int. Conf. Noise Fluctuations*, Jun. 2017, pp. 1–4.

[12] J. Andersen and R. Vaughan, "Transmitting, receiving, and scattering properties of antennas," *IEEE Antennas Propag. Mag.*, vol. 45, no. 4, pp. 93–98, Aug. 2003.

[13] D. M. Pozar, *Microwave Engineering*, 4th ed. Hoboken, NJ, USA: Wiley, 2012.

[14] W. Zhao and Y. Cao, "New generation of predictive technology model for sub-45 nm early design exploration," *IEEE Trans. Electron. Devices*, vol. 53, no. 11, pp. 2816–2823, Nov. 2006. [Online]. Available: http://ieeexplore.ieee.org/document/1715627/

[15] I. Khmyrova and Y. Seijyou, "Analysis of plasma oscillations in high-electron mobility transistorlike structures: Distributed circuit approach," *Appl. Phys. Lett.*, vol. 91, no. 14, 2007, Art. no. 143515.

[16] G. R. Aizin and G. C. Dyer, "Transmission line theory of collective plasma excitations in periodic two-dimensional electron systems: Finite plasmonic crystals and Tamm states," *Phys. Rev. B*, vol. 86, no. 23, Dec. 2012, Art. no. 235316.

[17] S. Preu *et al.*, "An improved model for non-resonant terahertz detection in field-effect transistors," *J. Appl. Phys.*, vol. 111, no. 2, 2012, Art. no. 024502.

[18] Y. Cheng and C. Hu, *MOSFET Modeling and Bsim3 User's Guide*. Norwell, MA, USA: Kluwer, 1999.
[19] M. Dyakonov and M. Shur, "Detection, mixing, and frequency multiplication of terahertz radiation by two-dimensional electronic fluid," *IEEE Trans. Electron. Devices*, vol. 43, no. 3, pp. 380–387, Mar. 1996.
[20] S. Boppel *et al.*, "CMOS integrated antenna-coupled field-effect transistors for the detection of radiation from 0.2 to 4.3 THz," *IEEE Trans. Microw. Theory Techn.*, vol. 60, no. 12, pp. 3834–3843, Dec. 2012.
[21] A. Lisauskas *et al.*, "Rational design of high-responsivity detectors of terahertz radiation based on distributed self-mixing in silicon field-effect transistors," *J. Appl. Phys.*, vol. 105, no. 11, 2009, Art. no. 114511.
[22] J. Zdanevičius *et al.*, "Camera for high-speed THz imaging," *J. Infrared, Millimeter, Terahertz Waves*, vol. 36, no. 10, pp. 986–997, Oct. 2015.
[23] P. Dean *et al.*, "Coherent three-dimensional terahertz imaging through self-mixing in a quantum cascade laser," *Appl. Phys. Lett.*, vol. 103, no. 18, Oct. 2013, Art. no. 181112.
[24] T. Hagelschuer *et al.*, "Terahertz gas spectroscopy through self-mixing in a quantum-cascade laser," *Appl. Phys. Lett.*, vol. 109, no. 19, Nov. 2016, Art. no. 191101.
[25] *Thz Golay cell detector datasheet for model sn190744*, Microtech Instruments Inc. Jun. 14, 2018. [Online]. Available: http://www.mtinstruments.com
[26] I. Kašalynas *et al.*, "Design and performance of a room-temperature terahertz detection array for real-time imaging," *IEEE J. Sel. Topics Quantum Electron.*, vol. 14, no. 2, pp. 363–369, Mar.–Apr. 2008.
[27] N. Oda, "Technology trend in real-time, uncooled image sensors for sub-THz and THz wave detection," *Proc. SPIE*, vol. 9836, May 25, 2016, Art. no. 98362P.
[28] M. Bolduc *et al.*, "Noise-equivalent power characterization of an uncooled microbolometer-based THz imaging camera," *Proc. SPIE*, vol. 8023, May 25, 2011, Art. no. 80230C.
[29] F. Simoens and J. Meilhan, "Terahertz real-time imaging uncooled array based on antenna- and cavity-coupled bolometers," *Philos. Trans. Roy. Soc. A: Math., Physical Eng. Sci.*, vol. 372, no. 2012, Feb. 2014, Art. no. 20130111.
[30] J. K. Choi *et al.*, "THz hot-electron micro-bolometer based on low-mobility 2-DEG in GaN heterostructure," *IEEE Sensors J.*, vol. 13, no. 1, pp. 80–88, Jan. 2013.
[31] D. Corcos *et al.*, "Antenna-coupled MOSFET bolometers for uncooled THz sensing," *IEEE Trans. Terahertz Sci. Technol.*, vol. 5, no. 6, pp. 902–913, Nov. 2015.
[32] A. Lisauskas *et al.*, "Exploration of terahertz imaging with silicon MOSFETs," *J. Infrared, Millimeter, Terahertz Waves*, vol. 35, no. 1, pp. 63–80, Jan. 2014.
[33] Z. Ahmad, A. Lisauskas, H. G. Roskos, and K. K. O, "9.74-THz electronic Far-Infrared detection using Schottky barrier diodes in CMOS," in *Proc. IEEE Int. Electron Devices Meeting*, San Francisco, CA, USA, Dec. 2014, pp. 4.4.1–4.4.4.
[34] A. Lisauskas *et al.*, "Terahertz rectification by plasmons and hot carriers in gated 2D electron gases," in *Proc. Int. Conf. Noise Fluctuations*, Xian, China, Jun. 2015, pp. 1–5.
[35] J. Vyšniauskas *et al.*, "Hydrodynamic modelling of terahertz rectification in AlGaN/GaN high electron mobility transistors," *J. Phys.: Conf. Ser.*, vol. 906, Oct. 2017, Art. no. 012023.
[36] A. Lee, B. Wil, S. Kumar, Q. Hu, and J. Reno, "Real-time imaging using a 4.3-THz quantum cascade laser and a 320 × 240 microbolometer focal-plane array," *IEEE Photon. Technol. Lett.*, vol. 18, no. 13, pp. 1415–1417, Jul. 2006.
[37] J. Trontelj *et al.*, "A high performance room temperature THz sensor," *Proc. SPIE*, vol. 9199, Sep. 5, 2014, Art. no. 91990K.

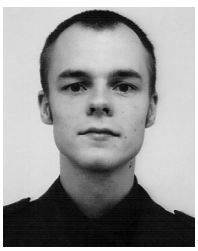

Justinas Zdanevičius was born in Alytus, Lithuania, in 1988. He received the M.S. degree in telecommunications physics and electronics from Vilnius University, Vilnius, Lithuania, in 2013.

His research interests include fluctuations and noise in electronic devices, CMOS THz detectors, and THz imaging.

Dovilė Čibiraitė received the B.S. degree in modern technologies physics and management and the M.S. degree in telecommunications physics and electronics from Vilnius University, Vilnius, Lithuania, in 2014 and 2016, respectively.

Her research interests include plasmonic THz detectors, such as graphene FET, silicon CMOS, and GaN HEMTs, and their further implementation for THz applications. Her research on THz rectification in monolayer graphene FETs led her to continue her research in THz radiation field.

Ms. Cibiraite was the recipient of the Marie Sklodowska-Curie Actions Grant to conduct her Ph.D. research on the topic of "THz camera based on GaN plasmonic FET devices" with the Department of Physics, Goethe University Frankfurt, Frankfurt, Germany, in 2016.

Kęstutis Ikamas (GS'18) received the diploma in physics from Vilnius University, Vilnius, Lithuania, in 1995, where he is currently working toward the Ph.D. degree in physics.

Since 2011, he has been a Lecturer with the Generolas Jonas Zemaitis Lithuania Military Academy, Vilnius. He is currently with the Noise and Terahertz Electronics Group, Vilnius University, where he is involved in CMOS-transistor-based THz design, modeling, and detection.

Maris Bauer was born in Frankfurt am Main, Germany, in 1985. He received the M.Sc. degree in physics from Goethe University Frankfurt, Frankfurt, Germany, for his work on inductive mesh bandpass filters for broadband THz spectroscopy, in 2012. From 2012 to 2017, he worked toward the doctoral degree at the Ultrafast Spectroscopy and Terahertz Physics Group, Goethe University Frankfurt, focusing on the modeling of charge carrier transport and photo-thermoelectric effects in TeraFETs and the implementation and characterization of devices in different materials, including novel carbon-based materials. He is currently waiting for the defense of his doctoral thesis.

From 2008 to 2014, he was with SynView GmbH, as a Research Assistant. He is currently with the Center for Materials Characterization and Testing, Fraunhofer ITWM, Kaiserslautern, Germany, working on THz applications and system design.

Jonas Matukas received the diploma degree in physics and doctoral degree from Vilnius University, Vilnius, Lithuania, in 1980 and 1993, respectively.

In 2000, he became an Associate Professor. Since 2008, he has been a Professor with the Radiophysics Department. Since 2013, he has been the Head of the Noise Research Laboratory, Vilnius University. His research interests include noise mechanisms and charge transfer in advanced optoelectronic and electronic devices with nanostructures (MQW laser diodes, avalanche photodetectors, new generation HBT transistors, CMOS FETs). He also contributes to the creation of terminology in the Lithuanian language in the fields of radiophysics, microelectronics, and electronics.

Alvydas Lisauskas (M'18) received the diploma degree in physics from Vilnius University, Vilnius, Lithuania, in 1995, and the Ph.D. degree from the Royal Institute of Technology, Stockholm, Sweden, in 2001.

In 2002, he was a Postdoc with the Ultrafast Spectroscopy and Terahertz Physics Group, Goethe University Frankfurt, Frankfurt, Germany, working on novel semiconductor devices for THz applications. Since 2014, he has been a Professor with Vilnius University and a leading Researcher with the Center for Physical Science and Technology, Vilnius. His research interests include THz electronics, design and modeling of semiconductor devices, and THz imaging techniques.

Heiko Richter received the diploma degree in physics from the Universität Karlsruhe, Karlsruhe, Germany, in 1999, and the Ph.D. degree in physics from the Technische Universität Berlin, Berlin, Germany, in 2005.

He is currently with the German Aerospace Center, Berlin, where he is involved in the field of THz and infrared sensors/optics.

Dr. Richter was the recipient of the Lilienthal Award for the development of a THz security scanner in 2007.

Till Hagelschuer received the M.Sc. degree in physics from Freie Universität, Berlin, Germany, in 2014. Since 2015, he has been working toward the Ph.D. degree at the Department of Optical Sensor Systems, Deutsches Zentrum für Luft- und Raumfahrt, Berlin.

His research interests include the application of external optical feedback phenomena in THz QCLs for high-resolution spectroscopy and imaging.

Viktor Krozer (M'91–SM'03) received the Dipl.-Ing. and Dr.-Ing. degrees in electrical engineering from Technical University (TU) Darmstadt, Darmstadt, Germany, in 1984 and 1991, respectively.

In 1991, he was a Senior Scientist with TU Darmstadt, working on high-temperature microwave devices and circuits and submillimeter-wave electronics. From 1996 to 2002, he was a Professor with the Technical University of Chemnitz, Chemnitz, Germany. From 2002 to 2009, he was a Professor with Electromagnetic Systems, DTU Elektro, Technical University of Denmark, and was heading the Microwave Technology Group. Since 2009, he has been an endowed Oerlikon-Leibniz-Goethe Professor of terahertz photonics with Goethe University Frankfurt, Frankfurt, Germany, and also heads the Goethe-Leibniz-Terahertz-Center, Goethe University Frankfurt. He is also with Ferdinand-Braun-Institut, Berlin, Germany, where he leads the THz components and systems group. His research interests include THz electronics, MMICs, nonlinear circuit analysis and design, device modeling, and remote sensing instrumentation.

Heinz-Wilhelm Hübers received the diploma and the doctoral degrees in physics from Universität Bonn, Germany, in 1991 and 1994, respectively.

From 1991 to 1994, he was with the Max-Planck-Institut für Radioastronomie, Bonn. In 1994, he joined Deutsches Zentrum für Luft- und Raumfahrt (German Aerospace Center, DLR), Berlin, Germany, and became the Head of Department in 2001. From 2009 to 2014, he was a Professor of experimental physics with the Technische Universität Berlin, Germany, and the Head of the Experimental Planetary Physics Department, DLR. In 2014, he was the Director of the Institute of Optical Sensor Systems, DLR, and a Professor with Humboldt-Universität zu Berlin. His research interests include THz physics and spectroscopy, particularly in THz systems for astronomy, planetary research, and security.

Dr. Hübers was the recipient of the Innovation Award on Synchrotron Radiation in 2003 and the Lilienthal Award in 2007.

Hartmut G. Roskos studied physics at the Technical University of Karlsruhe, Karlsruhe, Germany, and the Technical University of Munich, Munich, Germany. He received the Ph.D. degree from the Technical University of Munich, in 1989.

He is currently a Professor of physics with Johann Wolfgang Goethe-University, Frankfurt am Main, Germany. He was with AT&T Bell Laboratories, Holmdel, NJ, USA, where THz phenomena became the focus of his research. He joined the Institute of Semiconductor Electronics, RWTH Aachen, in 1991. After receiving the Habilitation degree with a thesis on coherent phenomena in solid-state physics investigated by THz spectroscopy, he became a Full Professor with Goethe University Frankfurt, Frankfurt, Germany, in 1997. He spent sabbaticals with the University of California at Santa Barbara, Santa Barbara, CA, USA, in 2005, and with the University of Rochester, Rochester, NY, USA, in 2014, and was an Invited Guest Professor with the Institute of Laser Engineering, Osaka University, during the 2009/2010 winter semester.

Dr. Roskos and his group was the recipient of a 5-year endowed professorship in 2009, which led to the establishment of a joint laboratory for THz photonics, awarded by OC Oerlikon AG jointly with the Ferdinand-Braun-Institute, Berlin, Germany. He is a Topical Editor for *Optics Letters*.